Comparative Study of Harmonic Response of Deep Groove Ball Bearing 6206 with Two and Three Surface-Defects

Shivam S. Dingane[a] S.S. Kinikar[b], Avdhut J. Gujar[c]
[a]*Head of Mechanical Engineering Department, Smt. Premalatai Chavan Polytechnic, Karad, Maharashtra, India*
[b]*Principal, Smt. Premalatai Chavan Polytechnic, Karad, Maharashtra, India*

Abstract: Vibration is one of the major parameters to consider in Monitoring health of rotating system. If an undetected fault is remains in the rotating system, it may result in break-down, huge damage, physical injury, or even cause death, therefore early fault identification is a critical factor in ensuring and extending the working life of the rotating systems. Bearings are the most critical components of any rotating system. Various sorts of vibrations occur in a rotor's mechanical system during operation, which frequently limits performance and endangers the operation's safety. However, it can also lead to downtime and costly damage if an undiagnosed problem is discovered in the rotating system. They are used to support rotating shafts. Thus, any flaw or malfunction in the factors might result in product position and outfit losses, as well as an unsafe working environment for humans. As a result, scholars have recently focused a lot of attention on address fault opinions. By vibration measurement and analysis of the bearing, it is possible to detect and locate important faults such as mass unbalance, misalignment, surface defects, and cracks. This article intends to provide researchers with guidance on how to apply vibration analysis for identifying, diagnosing, and addressing various common types of faults. It also highlights numerous essential techniques employed for this purpose condition monitoring of deep groove ball bearing such as fast Fourier transform, and FEM. This work focused on analyzing the modal and harmonic response of the Deep groove ball bearing with multiple surface defects.

Keywords: Deep Grove Ball Bearings; Finite Element Technique; Modal Analysis; Harmonic Analysis.

1. INTRODUCTION

Plain bearings for wheeled vehicles first appeared between 5000 BC and 3000 BC. The earliest known example of a rolling element bearing is a wooden ball bearing used in the spinning table of the Roman Nemi shipwreck, discovered in Lake Nemi, Italy, and dated to 40 BC. The first modern patent for ball bearings was granted to British inventor and iron master Philip Vaughan in 1794, who designed a ball bearing to support a carriage axle. Bearings are crucial components in any spinning system, as they provide support for rotating shafts in machinery. Faults or malfunctions in bearings can lead to production losses, equipment damage, and unsafe working conditions. Consequently, bearing fault diagnosis has gained significant research interest in recent years. Techniques such as time domain analysis, frequency domain analysis, and spike energy analysis are used to detect various bearing faults. Vibration is a key parameter in condition monitoring of rotating systems. Undetected faults can cause downtime, costly damage, injury, or even fatalities, making early fault identification essential for prolonging the life of rotating systems. Bearing failures can have extensive consequences, including increased downtime, high maintenance costs, missed deliveries, loss of revenue, and potential injuries to workers. Finite element analysis (FEA) uses calculations, models, and simulations to predict and understand how an object might behave under different physical conditions. Modal analysis determines a structure's vibration response, identifying natural or resonant frequencies both empirically and theoretically. These frequencies help determine the operational frequency range of a component. Harmonic Response Analysis, also known as Frequency Response Analysis, is a linear dynamic analysis used to assess a system's response to specific excitation frequencies. In this analysis, the load applied is a steady-state sinusoidal load at a given frequency, with possible phase differences between loads. The described Modal and Harmonic Response Analysis is performed on bearings with multiple surface defects at various operating speeds.Dipen S. Shah and colleagues [1] have aimed

to demonstrate the modeling and simulation of local and distributed defects on the inner and outer races of deep groove ball bearings. They modeled the bearing defect as an impulse train force or impact force to induce additional deflection or excitation of the rolling elements. The simulated results were analyzed in both the time and frequency domains. They thoroughly investigated the characteristic defect frequencies, their harmonics, and the amplitude of the vibration response of defective bearings using the simulation results.Suryawanshi G. L. and colleagues [2] examined the impact of inclined surface faults on the dynamic response of rolling element bearings. They derived a dynamic model using dimensional analysis. The vibration responses of double row spherical roller bearings were experimentally investigated to assess the effects of the size and slope angle of artificially created inclined surface faults. The results indicated that increasing the inclination angle of surface faults reduces the relative vibration amplitude at various rotor speeds, but the vibration amplitude increases with fault depth.Abhay Utpat [3] developed a model of a bearing as a spring-mass system, assuming the races as masses and the balls as springs. This work was further extended using Finite Element Analysis (FEA) to study the peaks at the defect frequencies of the bearing's outer and inner rings with artificial defects. Actual measurements of vibration amplitudes for bearings with these artificial local defects were conducted to verify the numerical results. The findings showed that the numerical results closely matched the experimental results. Standard support bearings were used throughout the experimentationV. N. Patel et al. [4,11] presented a dynamic model to study the vibrations of deep groove ball bearings with single and multiple defects on the inner and outer race surfaces. The model includes the masses of the shaft, housing, races, and balls. The coupled solutions of the governing equations of motion were obtained using the Runge-Kutta method. This model provides vibration responses of the shaft, balls, and housing in both time and frequency domains. The computed results were validated with experimental results from tests on healthy and defective deep groove ball bearings. Additionally, they performed theoretical and experimental vibration studies on dynamically loaded deep groove ball bearings with local circular defects on either race. The experimental setup used an electro-mechanical shaker to apply radial loads, with excitation frequencies ranging from 10 to 1000 Hz. The results from the mathematical model showed good agreement with the experimental findings.Laxmikant G Keni et al. [5] outlined a reliable procedure for precisely identifying defects in bearing components. The amplitude of vibrations was measured at 5000 RPM with a load of 200 N and for different defect sizes of 3 mm and 4 mm on the bearing races. An initial vibration analysis of a rolling component was performed using Ansys R-18.0. Vibration signals for the two different defect sizes were extracted, and an index for comparing various defect sizes was proposed. The study examined the effects of radial load, rotation speed, and initial defect size on stress levels.

Sameera Mufazzal et al. [6] presented an in-depth analysis of the vibration response of ball bearings using a modified 2-degree of freedom (DOF) lumped parameter model. This model incorporated additional deflection and multi-impact theories to closely simulate the behavior of healthy and defective bearings under different load and speed values. The researchers studied varying compliance vibration in detail and found that the location and number of impulses resulting from varying compliance strongly depended on multiple factors, primarily the values of applied load and shaft rotational speed. These impulses were observed to potentially merge with the actual defect-induced impulses, altering their characteristics. Numerical simulations were conducted at different speeds, loads, defect sizes, and locations to investigate the influence of these parameters on bearing response characteristics. Experimental results and detailed analyses were included in the paper to support the proposed model and validate the numerical findings.J Sopanen et al. [7,8] proposed a dynamic model of a deep-groove ball bearing with six degrees of freedom. This model encompassed descriptions of non-linear Hertzian contact deformation and elastohydrodynamic (EHD) fluid film. Input parameters such as geometry, material properties, and diametral clearance of the bearing were provided to the model. The calculation of bearing force and torque components relied on relative displacements and velocities between bearing rings. Both distributed defects, like inner and outer ring waviness, and localized defects, such as inner and outer ring defects, were accounted for in the model. In Part 1 of their study, the proposed ball bearing model was implemented and analyzed using a commercial multi-body system software application (MSC.ADAMS). The investigation focused on the impact of bearing diametral clearance

on the natural frequencies and vibration response of the rotor–bearing system. It was observed that the diametral clearance significantly influenced both the vibration level and natural frequencies. Low-order waviness, referred to as out-of-roundness, was identified to induce vibration at frequencies corresponding to the order of the waviness multiplied by the rotation speed. Conversely, waviness orders near the number of balls in the bearing (z ± 1 and z) generated vibrations at frequencies related to the ball passage inner ring and ball passage outer ring.TANG Zhaoping et al. [9] constructed a 3-D model of a deep groove ball bearing using the APDL language integrated into the finite element software ANSYS. Through contact analysis, they could visualize changes in stress, strain, penetration, sliding distance, and friction stress among the inner ring, outer ring, rolling elements, and cage. The simulation results indicated consistency between computational values and theoretical values. These findings collectively affirmed the correctness and rationality of the model and boundary conditions. They concluded that this model would furnish a scientific foundation for optimizing the design of rolling bearings under complex loads..Viramgama Parth D. et al. [12] conducted an analysis of ball bearings using finite element analysis to examine the stress levels and displacement behavior. The primary objective was to identify the most influential parameters affecting the radial stiffness of the bearing under axial loads. The study focused on a specific single row deep groove ball bearing with outer diameter 170 mm, inner diameter 80 mm, and ball diameter 28.575 mm. These bearings serve to support loads and facilitate relative motion within the mechanism. Through this analysis, they aimed to assess the bearing's lifespan, rejection rate, and productivity.Ghasem GhannadTehrani et al. [13] conducted a stability analysis of a ball bearing system considering varying stiffness coefficients. The presence of variable stiffness can lead to instabilities in the system at specific combinations of rotational speed, number, and dimensions of balls, thereby complicating the design process. The aim was to determine the stability boundary curves (SBCs) delineating stable and unstable regions. The well-known Mathieu equation was employed as the governing equations of the system in both horizontal and vertical directions. To calculate the SBCs, the equations of motion were solved using approximate methods such as the harmonic balance method (HBM) and the multiple scales method (MSM). While this process is straightforward for uncoupled Mathieu equations, either damped or undamped, a realistic bearing system necessitates consideration of two coupled Mathieu equations, introducing two dominant frequencies that are not integer coefficients of each other. For the first time, this set of damped and coupled equations applied to a bearing system was solved using HBM instead of relying on costly iterative methods. The accuracy of all investigated cases—uncoupled undamped, uncoupled damped, and coupled damped—was ensured through Floquet Theory.Iker Heras et al. [15] outlined the advantages of wire race bearings, including weight and inertia reductions, excellent shock load and vibration absorption capabilities, constant torque, and low maintenance requirements. Despite these benefits, there are limited wire race bearing manufacturers possessing the design and manufacturing expertise. This study aims to offer design guidelines for ball and crossed roller wire race bearings based on various geometrical parameters. The authors conducted a Design of Experiments (DoE) using Finite Element simulations to analyze the effects of these parameters on various performance indicators. The simulation results were meticulously compared to discern the impact of geometrical parameters on bearing performance.Wyatt Peterson et al. [14] utilized ANSYS FLUENT computational fluid dynamics (CFD) software to construct a comprehensive model of single-phase oil flow within a deep groove ball bearing (DGBB). The CFD model was employed to explore fluid flow characteristics concerning bearing geometry and operational conditions. The paper elaborates on the theoretical foundation, boundary conditions, and model development process. Through parametric studies, crucial aspects of the model such as meshing techniques, mesh density, and geometric clearances were determined. Streamlines, velocity vectors, and pressure contours were analyzed to investigate various aspects of DGBB behavior, including cage design and lubricant properties. The developed CFD model offers a novel approach for examining DGBB fluid flow dynamics and understanding the impact of cage geometry on bearing performance.

2. MODELING OF DEEP GROOVE BALL BEARING

The 3D model with two and three surface defects have been developed to analyze the frequency response and compare the results.

2.1 Bearing Specifications

Table No. 1 Dimensions of 6206 SKF deep groove ball bearing [15]

Dimensions	
Bore diameter (d)	30 mm
Outside diameter (D)	62 mm
Pitch Circle diameter	46 mm
Width (B)	16 mm
Roller diameter	10.4 mm
Ball Number	09
Mass of bearing	0.2kg

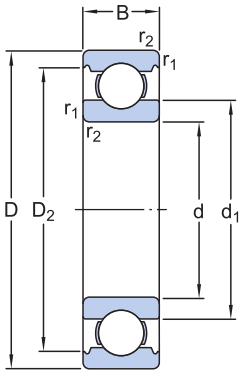

Figure 1. Illustrated Dimensions of 6206 Ball Bearing [15]

The whole bearing is made of Stainless steel, hence the properties of stainless steel are given below

Table No. 2Mechanical Properties of Stainless steel [16,17,18]

Properties	Value
Tensile Yield Strength(MPa)	207
Ultimate Yield Strength(MPa)	586
Density(kg/m3)	7750
Young's Modulus(MPa)	1.93E+05
Poisson's Ratio	0.31
Bulk Modulus(MPa)	1.693E+05

2.2 Geometric Model

The two 3-Dimensional geometric modelsare developed using Creo Parametric 5.0.6.0 with two and three surface-defects of 2x2x1 mm on the outside of inner race respectively.

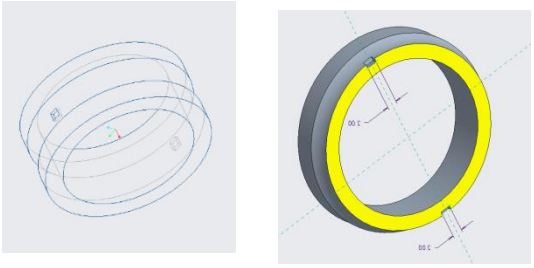

a b

Figure 2

Figure 2(a). Wireframe 3D model of inner race with two surface defects at an instant of 180º.

Figure 2(a). Section view of inner race.

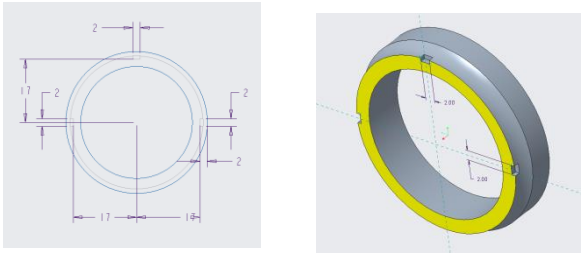

(a) (b)

Figure 3

Figure 3(a). Wireframe 3D model of inner race with three surface defects at an instant of 90º.

Figure 3(b). Section view of inner race.

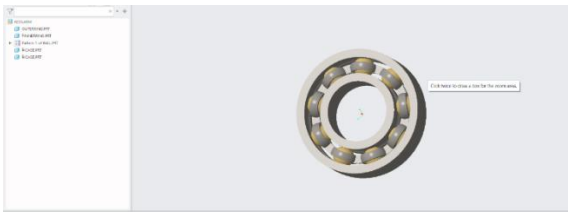

Figure 4. 3D Model of Deep Groove Ball bearing

The above figure shows the complete assembly of deep groove ball bearing which includes Outer race, Inner race with two and three defects, balls and cage. The model will be used to perform frequency response analysis.

2.3 Rotar Dynamics Equation

The General equation is given by

$$[\boldsymbol{M}]\{\ddot{\boldsymbol{\mu}}\} + [\boldsymbol{c}]\{\dot{\boldsymbol{\mu}}\} + [\boldsymbol{K}]\{\boldsymbol{\mu}\} = \{\boldsymbol{f}(\boldsymbol{t})\} \quad (1)$$

[M], is the mass matrix [C], is the damping matrix and [K] is the stiffness matrix, and {f} is the external vector force, In the rotor dynamics, this equation gets additional contributions from the gyroscopic effect [G], and the rotating damping effect [B] leading:

$$[\boldsymbol{M}]\{\ddot{\boldsymbol{\mu}}\} + ([\boldsymbol{C}] + [\boldsymbol{G}]\{\dot{\boldsymbol{\mu}}\}) + ([\boldsymbol{K}] + [\boldsymbol{B}])\{\boldsymbol{\mu}\} = \{\boldsymbol{F}(\boldsymbol{t})\} \quad (2)$$

In modal analysis the mode shapes and natural frequencies with them are one of the characteristics of the mechanical structure, regardless of any loads, what we do is an undamped vibration system, so the external excitation and damping are not taken into account in the model analysis, and from it, the equation (2) can be simplified as follows:

$$[\boldsymbol{M}]\{\ddot{\boldsymbol{\mu}}\} + ([\boldsymbol{K}] + [\boldsymbol{B}])\{\boldsymbol{\mu}\} = \{\boldsymbol{0}\} \quad (3)$$

The free vibration of an elastic body can always be decomposed into a series of simple harmonic vibrations, that is, it can be assumed that each point in the structure experiences a harmonic motion that can decrease due to frequency, amplitude, and phase angle. The equation is simplified to:

$$(([\boldsymbol{K}] - [\boldsymbol{B}]) - \boldsymbol{\omega_i^2}[\boldsymbol{M}])\{\emptyset\}_{\boldsymbol{i}} = \boldsymbol{0} \quad (4)$$

is the eigenvalue, is the eigenvector, So, the equation for free vibration becomes:

$$\left|([\boldsymbol{K}] - [\boldsymbol{B}]) - \boldsymbol{\omega_i^2}[\boldsymbol{M}]\right)| = \boldsymbol{0} (5)$$

is the natural frequency of the mode shape.

For harmonic response the equation of forced vibration is given by:

$$[\boldsymbol{M}]\{\ddot{\boldsymbol{\mu}}\} + [\boldsymbol{c}]\{\dot{\boldsymbol{\mu}}\} + [\boldsymbol{K}]\{\boldsymbol{\mu}\} = \{\boldsymbol{f}(\boldsymbol{t})\} (6)$$

$$\boldsymbol{f}(\boldsymbol{t}) = \boldsymbol{f_0} \sin \boldsymbol{\omega t} \ (7)$$

3. FINITE ELEMENT MODEL

The Ansys R1 workbench software is used to perform finite element modelling and obtaining the results in the form of mode shapes and Campbell diagram [19,20]

3.1 Boundary Conditions

The same boundary conditions are applied to both the models with 2 and 3 surface-defects.

3.1.1 Connections and Joints

The connections of the components of the ball bearing which includes the contact between balls and outer race and balls and inner race. By considering Ideal condition these contacts are defined are frictionless.

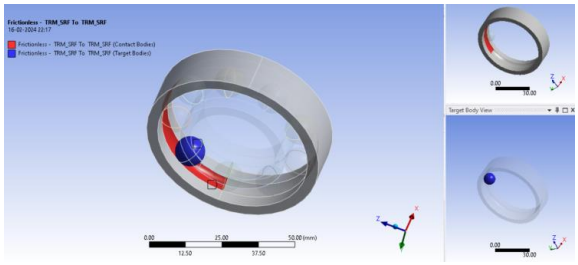

Figure 5 – Contact between anyone ball and outer race

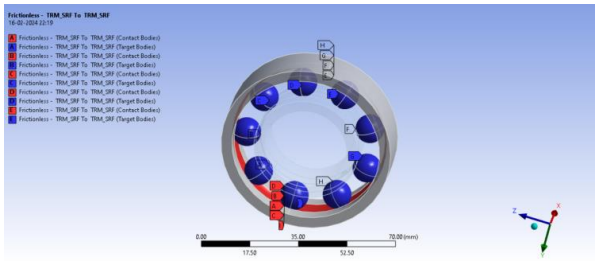

Figure 6 – Contact between the balls and outer race

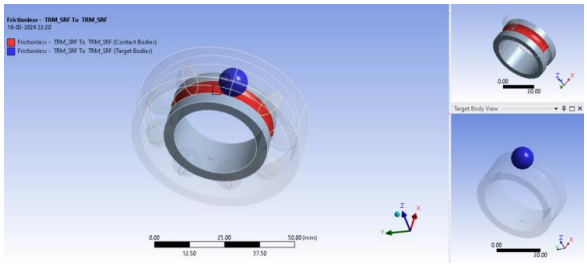

Figure 7 – Contact between anyone ball and inner race

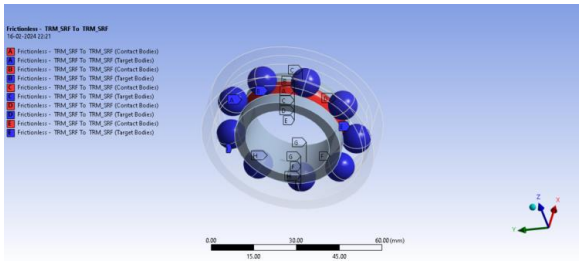

Figure 8 – Contact between the balls and inner race

The total number of 18 frictionless connections are defined where nine connections are between balls and outer and other nine connections are between balls and inner race.

The joints between the components of deep groove ball bearing are also defined in the connection tab, the revolute joint is defined for the inner race and balls where it permits rotation only in one direction i.e., Z.

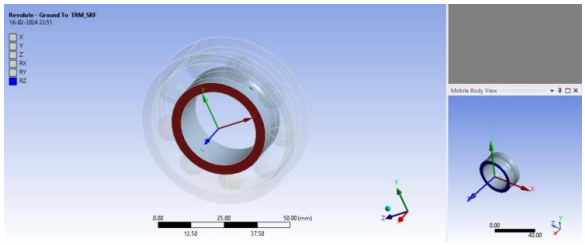

Figure 9 – Inner race defined as revolute joint

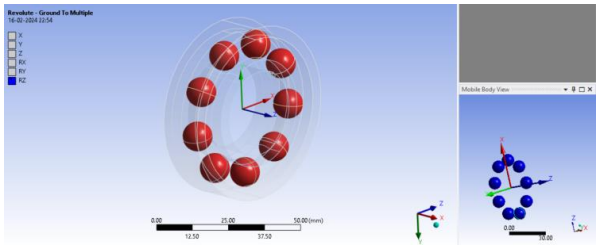

Figure 10 – Bearing balls defined as revolute joint

3.1.2 Boundary Conditions for Modal Analysis

We provide the condition of remote displacement to the ball bearing location to constraint the motion of bearing in the Z axis direction, the translation degrees of freedom are also restricted in the direction of Z axis.

The given maximum speed of bearing is 15000 rpm and the reference speed of bearing is 24000 rpm (revolutions per minute) [15] as per SKF bearing specifications. The modal analysis is carried out in three steps with three different speeds of 2000, 15000 &24000rpm for obtaining mode shapes and Campbell Diagram.

The outer race is considered as fixed support where actually the bearing is mounted or fixed, and the rotational velocity is provided to the inner race where it is mounted on shaft.

Analysis Setting are as follows- 4 number of modes to find and the solution system used is damped solver with full damped type and Coriolis effect turned on also Campbell diagram with 3 number of points.

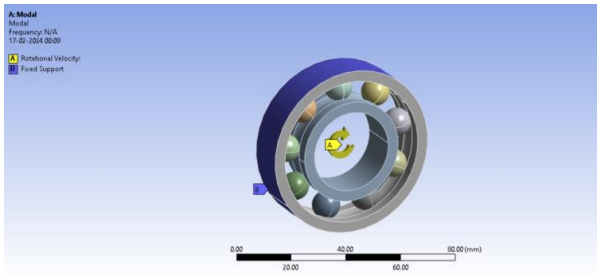

Figure 11 – Rotating velocity and fixed support applied

3.1.3 Boundary Conditions for Harmonic Response

We use the condition of remote displacement to the deep groove ball bearing where the constraint is put on the rotational and transition degrees of freedom in the direction of the Z-axis at bearing sites

The fixed support is applied to the outer race whereas the rotational velocity is provided to the inner race. The rotational velocity (in rpm) is converted to Relative Centrifugal force (RCF in Newtons). The conversion is given by

$$\boldsymbol{RCF} = \mathbf{1.12} \times \boldsymbol{r}\,(\boldsymbol{RPM}/\mathbf{1000})^2 \quad (8)$$

Where RCF is the Relative Centrifugal force and r is the radius of rotating component.

Therefore, to obtain the speed of 2000 rpm, the equation no. 8 is modified according to the values of the bearing

$$\therefore \boldsymbol{RCF} = \mathbf{1.12} \times \mathbf{15}\,(\mathbf{2000}/\mathbf{1000})^2 \quad (9)$$

$$\therefore \boldsymbol{RCF} = \mathbf{67.2}\,\boldsymbol{N} \quad (10)$$

The RCF of 67.2N is applied to the inner race at the remote point created for the location of hit point.

In the analysis settings the frequency range were defined from 0 to 2000 Hz with 100 solution intervals

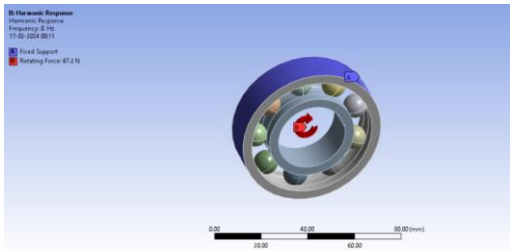

Figure 12 – Appliedrotating force and fixed support applied

3.1.4 Meshing

ANSYS's meshing method plays an essential role for accurate simulation utilizing Finite Element Analysis (FEA). The mesh is made up of elements with nodes that represent the shape of the geometry and can vary depending on the element type. FEA reduces degrees of freedom from unlimited to limited by performing calculations at a finite number of elements and interpolating the results to the full size of a continuous object. The ANSYS workbench offers a variety of meshing methods, including mechanical.

The average surface area covered 307.32 mm². A total number of 3158 elements are created and 7746 nodes are shown in the below figure.

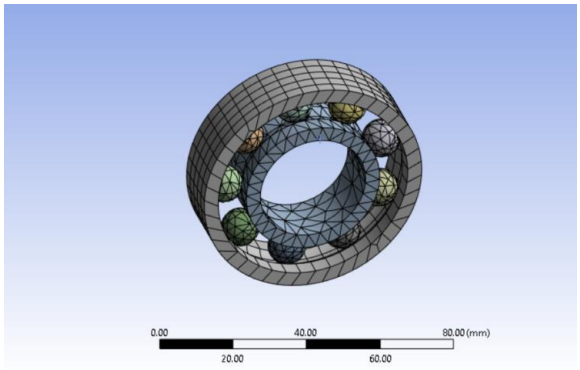

Figure 13 – Bearing Mesh

4. RESULTS

4.1 Modal Analysis of Ball Bearing with 2 Surface-Defects

Modal analysis was carried out for deep groove ball bearing with two surface defects. Where we note that first natural frequency is 771.61 Hz and natural frequency at second mode is almost twice the first i.e., 1588.6 Hz.

4.1.1 Mode Shapes

Total 4 mode shapes are generated with full damped type solver as follows.

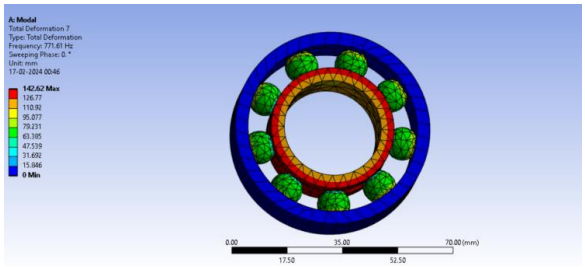

Figure 14 (a)– Mode Shape 1

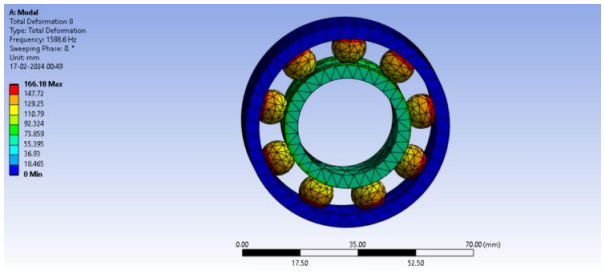

Figure 14 (b)– Mode Shape 2

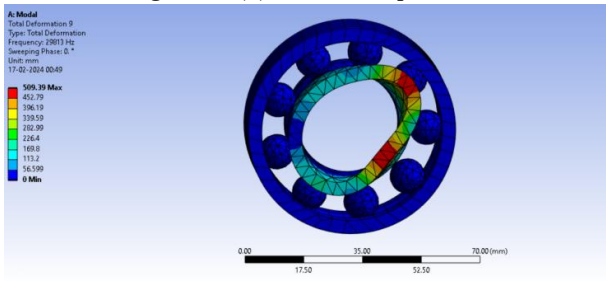

Figure 14 (c)– Mode Shape 3

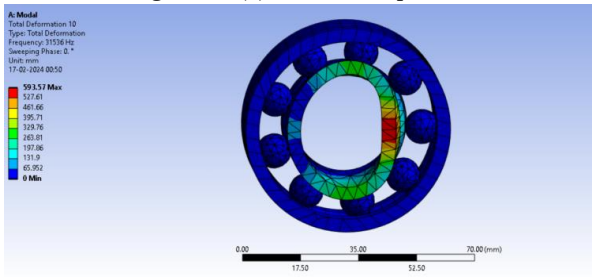

Figure 14 (d)– Mode Shape 4

4.1.2 Campbell Diagram

We can obtain Campbell diagram as shown in Fig 15 to analyze the evolution of frequencies at the speed of rotation and to determine the critical velocities and stability threshold.We note that there isone critical speed of 15432 rpm at 771.61 Hz, and the mode stability is stable.

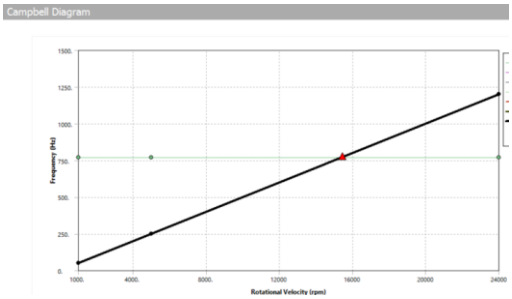

Figure 15 – Campbell Diagram

4.2 Modal Analysis of Ball Bearing with 3 Surface-Defects

Modal analysis for deep groove ball bearings with three surface-defects were carried out. Where the natural frequencies at first two modes are 772.95 Hz and 1591.7 Hz respectively. As compared with previous results we can clearly see the natural frequencies are slightly increased than the natural frequencies of bearing with two surface defects.

4.2.1 Mode Shapes

In general, 4 mode shapes are generated with full damped type solver shown in Fig 16(a), 16(b), 16(c) and 16(s)

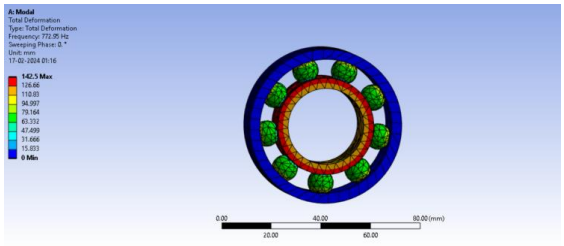

Figure 16 (a)– Mode Shape 1

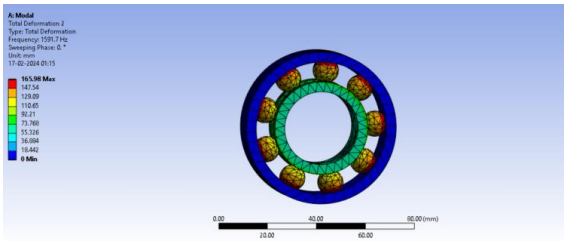

Figure 16 (b)– Mode Shape 2

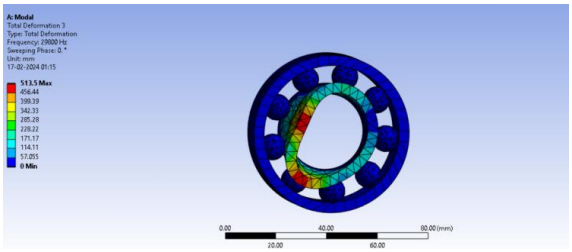

Figure 16 (c)– Mode Shape 3

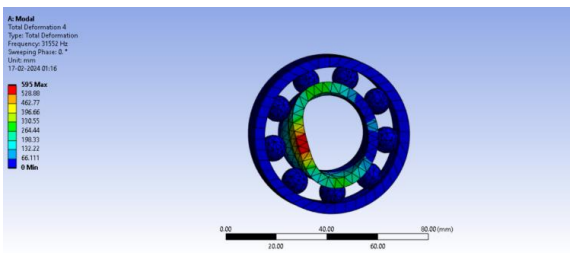

Figure 16 (d)– Mode Shape 4

4.2.2 Campbell Diagram

The Campbell diagram is obtained as given the in Fig 17Where we note that there isone critical speed of 15459 rpm at 772.95 Hz, and the mode stability is stable. As compared with the results of analysis of bearing with two surface defects we can observer slight increment in the critical speed at natural frequency.

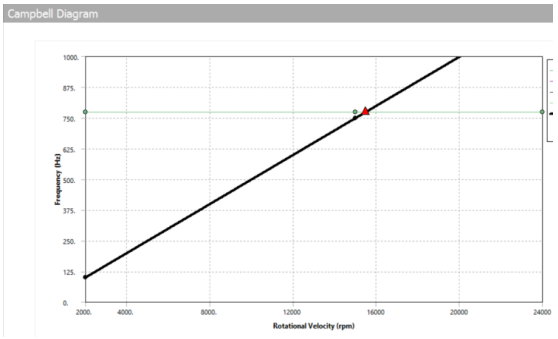

Figure 17– Campbell Diagram

4.3 Harmonic Response Analysis Ball Bearing with 2 Surface-Defects

The harmonic response analysis of the system scope us to determine the deformation, stresses, and effect of phase angle due to balanced and unbalanced forces acting on the bearing system, The harmonic analysis was carried out to show the frequency response by applying anRelative centrifugal force of 67.2 N converted in equation number (10) generated due to angular velocity of 2000 rpm.

4.3.1 Frequency Response

The frequency response was plotted on the graph with frequency ranged from 0 Hz -1000 Hz on X-axis and three different amplitudes (mm, m/s, m/s^2) on Y-axis individually is given below

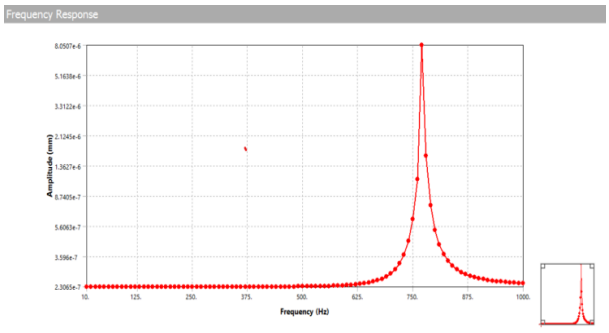

Figure 18 (a)– Frequency Response Hz vs. mm

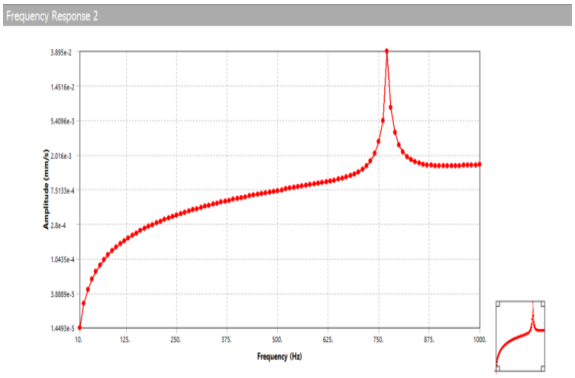

Figure 18 (b)– Frequency Response Hz vs. m/s

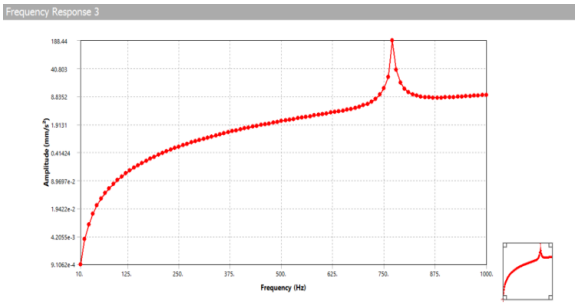

Figure 18 (c)– Frequency Response Hz vs. m/s^2

From figure 18 (a, b, c) we noted that the maximum deflection that is amplitude in mm, m/s and m/s^2 occurs at the frequency of 770 Hz.

4.3.2 Phase Response

Phase response is calculated to find the effect of phase angle on deformation. The phase angle reported is 106.88^o at frequency of 770Hz as shown in figure below

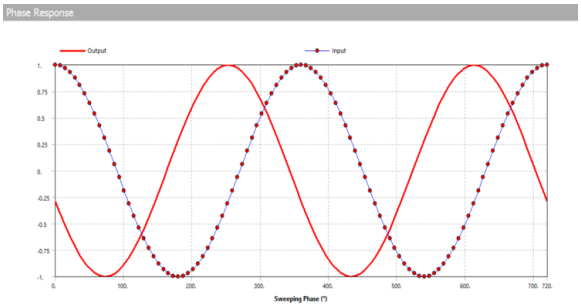

Figure 19– Phase Response

4.4 Harmonic Response Analysis Ball Bearing with 3 Surface-Defects

The harmonic response analysis of the system is carried out to determine the deformation, stresses, and effect of phase angle due to balanced and unbalanced forces acting on the bearing system, The harmonic analysis was carried out to obtain the frequency response by applying aRelative centrifugal

force of 67.2 N converted in equation number (10) generated due to angular velocity of 2000 rpm.

4.4.1 Frequency Response

The frequency response was mentioned on the graph with frequency ranged up to 1000 Hz on X-axis with three different amplitudes (mm, m/s, m/s^2) on Y-axis as shown in figures below in detail. We recorded the maximum amplitude on the frequency of 780 Hz.

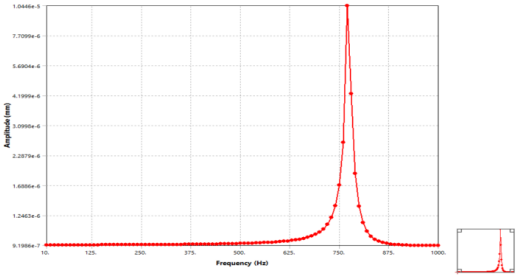

Figure 20 (a)– Frequency Response Hz vs. mm

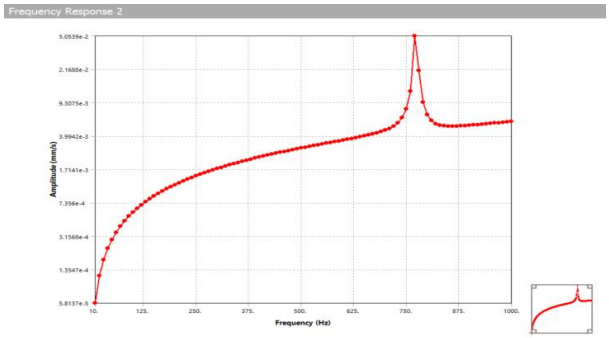

Figure 20 (b)– Frequency Response Hz vs. m/s

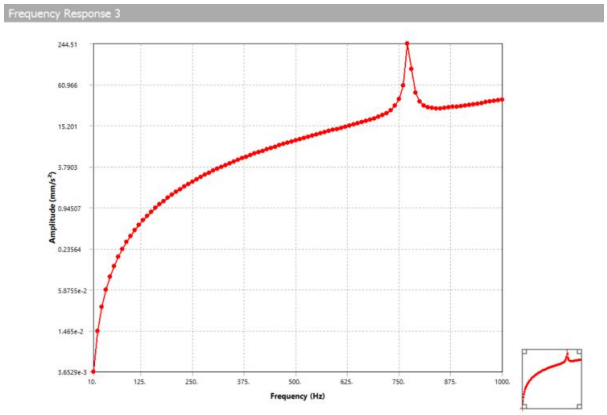

Figure 20 (c)– Frequency Response Hz vs. m/s^2

4.4.2 Phase Response

Phase response is plotted to see the effect of phase angle on the deformation. The angle reported is -87.41^o at the frequency of 780Hz.

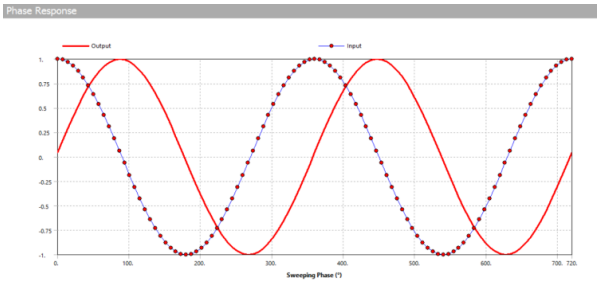

Figure 21 – Phase Response

5. CONCLUSION

In this research we have carried out the dynamic analysis of deep groove ball bearing with two and three surface defects cause due to improper lubrication, contamination and dirt. We Developed 3D model of deep groove ball bearing using Creo Parametric 5.0.6.0 and performed Modal and Harmonic response analysis using Ansys workbench. We obtained the mode shapes, Campbell diagram in modal analysis and Frequency response analysis and phase response in Harmonic analysis for two and three surface-defects on deep groove ball bearing and it was obtained:

- The frequencies of first two modes in the bearing with two surface-defects were 771.61 Hz and 1588.6 Hz respectively, that of natural frequencies of the bearing with 3 surface defects were 772.95 Hz. And 1591.7 Hz where we can clearly observer slight increment in both. Whereasin the Campbell diagram we noticed the critical speed of 15432 rpm at the frequency of 771.61 Hz in the bearing with two surface defects and the critical speed of 15459 rpm was noted at the frequency of 772.95 Hz in the bearing with 3 Surface-defects.
- In the harmonic response analysis, we have note that the maximum deflection (deformation in mm, velocity in m/s and acceleration in m/s^2) is obtained at the frequency of 770 Hz in the bearing with 2 surface defects and the phase angle plotted is 106.88^o at 770 Hz. Whereas the maximum amplitude obtained in ball bearing with 3 surface defects were at the frequency of 780 Hz, and phase angle plotted at -87.41^o at the frequency of 780 Hz.

REFERENCES

[1]. Dipen S. Shah, V. N. Patel “Study on Excitation Forces Generated by Defective Races of Rolling Bearing” Procedia Technology 23 (2016) 209 – 216.

[2]. Ganesh L. Suryawanshi, Sachin K. Patil , Ramchandra G. Desavale, "Dynamic model to predict vibration characteristics of rolling element bearings with inclined surface fault" Department of Mechanical Engineering, Rajarambapu Institute of Technology, Rajaramnagar, Shivaji University, Kolhapur 415414, Maharashtra, India.

[3]. Abhay Utpat "Vibration Signature analysis of defective deep groove ball bearings by Numerical and Experimental approach" International Journal of Scientific & Engineering Research, Volume 4, Issue 6, June-2013 592 ISSN 2229-5518.

[4]. V. N. PatelN. TandonR. K. Pandey, "A Dynamic Model for Vibration Studies of Deep Groove Ball Bearings Considering Single and Multiple Defects in Races" Industrial Tribology, Machine Dynamic, and Maintenance Engineering Centre (ITMMEC), IIT Delhi, New Delhi 110 016, India.

[5]. Laxmikant G Keni, Padmaraj N H, Najiullah Khan, Jagadeesha P E, Pradeep R, Chethan K N "ANALYSIS OF VIBRATION SIGNATURE IN DEEP GROOVE BALL BEARING USING FINITE ELEMENT METHOD" Paper number: 20(2022)3, 992, 861-869.

[6]. Sameera Mufazzal, SM Muzakkir, Sidra Khanam "Journal of Sound and Vibration 513 (2021) 116407 Available online 19 August 2021 0022-460X/© 2021 Elsevier Ltd. All rights reserved.Theoretical and experimental analyses of vibration impulses and their influence on accurate diagnosis of ball bearing with localized outer race defect" Journal of Sound and Vibration 513 (2021) 116407.

[7]. J Sopanen and A Mikkola "Dynamic model of a deep-groove ball bearing including localized and distributed defects. Part 1" DOI: 10.1243/14644190360713551

[8]. J Sopanen and A Mikkola "Dynamic model of a deep-groove ball bearing including localized and distributed defects. Part 2" DOI: 10.1243/14644190360713560

[9]. TANG Zhaopinga, SUN Jianping "The Contact Analysis for Deep Groove Ball Bearing Based on ANSYS" 1877-7058 © 2011 Published by Elsevier Ltd. doi:10.1016/j.proeng.2011.11.2524

[10]. Putti Srinivasa Rao, NariseSaralika, "Thermal and Vibration Analysis of 6200 Deep Groove Ball Bearing" SSRG International Journal of Mechanical Engineering (SSRG-IJME), ISSN: 2348 – 8360.

[11]. V. N. Patel, N. Tandon, R. K. Pandey, "Vibration Studies of Dynamically Loaded Deep Groove Ball Bearings in Presence of Local Defects on Races" Procedia Engineering 64 (2013) 1582 – 1591

[12]. Viramgama Parth D. "Analysis of Single Row Deep Groove Ball Bearing", International Journal of Engineering Research & Technology (IJERT)

[13]. G.G. Tehrani, C. Gastaldi and T.M. Berruti, Stability analysis of a parametrically excited ball bearing system, International Journal of Non-Linear Mechanics (2019), doi: https://doi.org/10.1016/j.ijnonlinmec.2019.103350.

[14]. Peterson W, Russell T, Sadeghi F, Berhan MT, Stacke L-E, Ståhl J, A CFD Investigation of Lubricant Flow in Deep Groove Ball Bearings, Tribology International, (2020), doi: https://doi.org/10.1016/j.triboint.2020.106735.

[15]. SKF Deep Groove Ball bearing 6206, doi:https://www.skf.com/group/products/rolling-bearings/ball-bearings/deep-groove-ball-bearings/productid-6206

[16]. H. Huang, Z. Yuan, W. Kang, Z. Xue, X. Chen, C. Yang, Y. Ye, J. Leng, Study of the sealing performanceof tubing adapters in gas-tight deep-sea water sampler, Int. J. Nav. Archit. Ocean Eng. 6 (2014) 749–761.doi:10.2478/IJNAOE-2013-0212.

[17]. M.B. Davanageri, S. Narendranath, R. Kadoli, Finite Element Wear Behaviour Modelling of Super duplex stainless steel AISI 2507 Using Ansys, IOP Conf. Ser. Mater. Sci. Eng. 376 (2018). doi:10.1088/1757899X/376/1/012131.

[18]. L. Gardner, The use of stainless steel in structures, Prog. Struct. Eng. Mater. 7 (2005) 45–55.doi:10.1002/pse.190.

[19]. Grunwald, B., Vibration analysis of shaft in SolidWorks and ANSYS. 2018.

[20]. Mansoora, H.I., M. Al-Shammari, and A. Al-Hamood. Theoretical Analysis of the Vibrations in Gas Turbine Rotor. in IOP Conference Series: Materials Science and Engineering. 2020. IOP Publishing